Deformation-Induced Changes in Hydraulic Head During Ground-Water Withdrawal

by Paul A. Hsieh[a]

Abstract

Ground-water withdrawal from a confined or semiconfined aquifer causes three-dimensional deformation in the pumped aquifer and in adjacent layers (overlying and underlying aquifers and aquitards). In response to the deformation, hydraulic head in the adjacent layers could rise or fall almost immediately after the start of pumping. This deformation-induced effect is analyzed by a linear poroelasticity model using properties typical of unconsolidated sedimentary materials. Model simulations suggest that an adjacent layer undergoes horizontal compression and vertical extension when pumping begins. Hydraulic head initially drops in a region near the well and close to the pumped aquifer, but rises outside this region. Magnitude of head change varies from a few centimeters to more than 10 centimeters. Factors that influence the development of deformation-induced effects includes matrix rigidity (shear modulus), the arrangement of aquifer and aquitards, their thicknesses, and proximity to land surface. Induced rise in hydraulic head is prominent in an aquitard that extends from land surface to a shallow pumped aquifer. Induced drop in hydraulic head is likely observed close to the well in an aquifer that is separated from the pumped aquifer by a relatively thin aquitard. Induced effects might last for hours in an aquifer, but could persist for many days in an aquitard. Induced effects are eventually dissipated by fluid flow from regions of higher head to regions of lower head, and by propagation of drawdown from the pumped aquifer into adjacent layers.

Introduction

It is well-documented that when ground water is pumped from a confined or semiconfined aquifer, hydraulic head in adjacent aquifers and aquitards could rise or fall almost immediately after the start of pumping. The onset of these responses occurs much earlier than the hydraulic propagation of drawdown from the pumped aquifer into adjacent layers. An initial rise in hydraulic head in adjacent layers is commonly called "reverse water-level fluctuation" (Andreason and Brookhart, 1963) or "Noordbergum effect," so named because it was first observed at the village of Noordbergum in the Netherlands (Verruijt, 1969, p. 368). An initial drop in hydraulic head has also been observed. Ferris et al. (1962, p. 80) report cases in which "a well screened in the upper aquifer . . . is pumped and the water level in the well screened in the lower aquifer abruptly declines when pumping begins. As pumping continues, the water level of the lower aquifer ceases to decline and gradually recovers its initial position." Data published by Wolff (1970a, Figure 9) show both initial rise (up to about 26 cm) and drop (by about 6 cm) in hydraulic head at different depths in a clay bed underlying a pumped aquifer. Wolff (1970b, Figure 8) also cites observation of a 7-cm rise in hydraulic head in an unpumped aquifer that is separated from an underlying pumped aquifer by a clay bed.

The rapid response of hydraulic head in layers adjacent to the pumped aquifer is commonly attributed to three-dimensional deformation induced by pumping. Accompanying the release of water from compressive storage is a decrease in aquifer volume. This volume reduction occurs as both horizontal and vertical strains. These strains will, in turn, induce deformations in adjacent layers. Wolff (1970b, p. 1721) attributes head rise in adjacent layers to "distortion of the pore space . . . resulting from the transference of horizontal strain from the aquifer via shear." To explain the abrupt drop in hydraulic head, Ferris et al. (1962, p. 80) reason that vertical contraction of the pumped aquifer would cause "bowing" of adjacent layers, creating additional water storage space and thereby lowering hydraulic head. In both cases of head rise and head drop, the driving mechanism is deformation of the pumped aquifer. In the present study, the two effects are collectively referred to as "deformation-induced effects."

Although the above explanation of deformation-induced effects appears well accepted, quantitative analyses of the phenomenon are few. Three factors could explain the paucity of studies. First, hydraulic heads in adjacent aquitards and unpumped aquifers are not routinely monitored during aquifer tests. As a result, deformation-induced effects often go unobserved. Second, the magnitude of deformation-induced head change is typically less than a few tens of cm, and the effect is reversed when drawdown in the pumped aquifer propagates into adjacent layers. If drawdowns reach meters or tens of meters at later times, deformation-induced effects at early times are often ignored in aquifer-test analysis. Third, a three-dimensional analysis of fluid flow coupled with aquifer deformation requires a poroelasticity (Biot) theory, which is considerably more complex than conventional ground-water theory. Except for simple cases, poroelasticity equations are not analytically tractable. To solve these equations, previous investigations (Verruijt, 1969; Wolff, 1970b; and Gambolati, 1974) introduce numerous simplifying assumptions to the extent that the results are useful primarily as qualitative indications. Analysis of realistic aquifer settings generally requires a numerical poroelasticity model. This type of model is not well-known to most ground-water hydrologists.

The purpose of the present study is to quantitatively analyze deformation-induced effects during ground-water withdrawal.

[a]U.S. Geological Survey, 345 Middlefield Road, Mail Stop 496, Menlo Park, California 94025.

Received June 1995, revised November 1995, accepted December 1995.

Such an analysis is, in itself, an interesting application of poroelasticity theory. From a practical point of view, a quantitative understanding of the phenomenon would provide improved guidelines for analyzing drawdown in aquifers and aquitards adjacent to the pumped aquifer. Analysis of coupled flow and deformation during pumping might also yield estimate of parameters (elastic moduli) useful to studies of three-dimensional compaction and subsidence.

The rest of this paper begins by summarizing the key features of linear poroelasticity theory. A numerical model is then used to analyze deformation-induced effects in two aquifer settings. The first setting focuses on head changes in aquitards, whereas the second setting focuses on head changes in unpumped aquifers. Factors that influence deformation-induced effects are examined by varying model parameters.

Linear Poroelasticity Theory

Since the pioneering work of Biot (1941), linear poroelasticity theory has been a valuable method for analyzing interaction between fluid flow and skeletal-matrix deformation. In this theory, fluid flow obeys Darcy's Law and mass conservation. Matrix deformation obeys Biot's constitutive relations and stress equilibrium. Strains are assumed to be small. The general theory allows both fluid and grains to be compressible. Details of linear poroelasticity theory can be found in numerous publications in the soil and rock mechanics literature (see, for example, the review article by Detournay and Cheng, 1993). The discussion by Verruijt (1969) is particularly useful to the present study because it analyzes problems associated with ground-water withdrawal from wells.

The central difference between poroelasticity theory and conventional ground-water theory lies in the treatment of matrix deformation. Conventional ground-water theory assumes no horizontal displacement of the matrix, and a constant vertical component of total stress. Under this assumption, fluid flow can be decoupled from matrix deformation, making it possible to solve for hydraulic head by itself. In contrast, poroelasticity theory allows the skeletal matrix to deform in three dimensions, and vertical stress need not remain constant. In this more general approach, matrix deformation and fluid flow are coupled to each other. The solution of poroelasticity equations requires simultaneously solving for head and displacement.

In the present study, four simplifications are made to model typical well problems in aquifer-aquitard systems. First, the subsurface is in an initial state of hydraulic and mechanical equilibrium. This means that variables in the poroelasticity equations can be formulated in terms of their departures from the initial state. Second, drawdown of the water table is small and can be neglected. This is a limitation of the present analysis, but is reasonable if the water table is in an aquitard that overlies the pumped aquifer, or in an aquifer that is separated from the pumped aquifer by an aquitard. Third, grains are incompressible, but fluid is compressible. This assumption is reasonable for unconsolidated sediments and is consistent with conventional ground-water theory. Finally, physical properties are isotropic and homogeneous within an aquifer or an aquitard. This assumption limits the number of physical properties to a manageable quantity in the analysis.

Under the above assumptions, the governing equations of linear poroelasticity are (Verruijt, 1969, p. 342)

$$K\nabla^2 h = \frac{\partial}{\partial t}(\nabla \cdot \underline{u}) + \rho_f g n \beta \frac{\partial h}{\partial t} \quad (1)$$

$$G\nabla^2 \underline{u} + \frac{G}{1 - 2\nu} \nabla (\nabla \cdot \underline{u}) - \rho_f g \nabla h = 0 \quad (2)$$

where h is change in hydraulic head, $\underline{u}$ is displacement (change in position) of the skeletal matrix, K is hydraulic conductivity, n is porosity, $\rho_f g$ and β are respectively the specific weight and compressibility of fluid, and G and ν are respectively the shear modulus and drained Poisson's ratio of the skeletal matrix. The mechanical properties G and ν are related to the vertical matrix compressibility, usually denoted by in the ground-water texts (for example, Freeze and Cherry, 1979, p. 54), by

$$\alpha = \frac{1 - 2\nu}{2G(1 - \nu)} \quad (3)$$

Note that (3) implies that for a fixed Poisson's ratio, a stiffer matrix (higher G) is also less compressible (lower α). For fully three-dimensional problems, (2) consists of three component equations, so (1) – (2) together form a set of four equations in four unknowns. For axisymmetric problems, such as flow to a well, (1) – (2) reduce to three equations in three unknowns (h and the radial and vertical components of $\underline{u}$).

Two types of boundary conditions—hydraulic and mechanical—must be specified at each boundary. Hydraulic boundary conditions are similar to those in conventional ground-water theory, except they are formulated here in terms of changes from the initial state. Typical hydraulic boundary conditions are specified change in head and specified change in flux. (A water-table boundary is not yet implemented in the numerical code.) Mechanical boundary conditions are similar to those in elasticity theory. They are either specified displacement or specified change in boundary traction (applied stress).

Except for simple cases, solution of (1) – (2) requires numerical methods. Finite-element solution of (1) – (2) is extensively applied in soil-compaction and land-subsidence analyses (Sandhu, 1979). For this study, a numerical model is developed following the finite-element solution method of Smith and Griffiths (1988, Chapter 9). In this formulation, material properties are assumed uniform within each element, but properties may vary from one element to the next. Therefore, the model may be applied to solve problems with nonuniform distribution of properties, including layered aquifer-aquitard systems. The model has been tested for accuracy by comparison with analytical solutions derived by McNamee and Gibson (1960), Schiffman et al. (1969), Gibson et al. (1970), and Geerstma (1973). In every test case, the numerical solution closely matched the analytical solution.

Deformation-Induced Effects in Aquitards

Figure 1 shows a hypothetical setting consisting of a 100-m thick, laterally extensive aquifer that is confined above and below by aquitards. The upper aquitard is also 100 m thick, and the lower aquitard extends to a great depth. The water table coincides with the land surface, which is the top of the upper aquitard. A well is drilled through all three units, is cased throughout both aquitards, and is screened over the entire thickness of the aquifer. Ground water is pumped at a constant rate of 5×10^{-2} m^3/s (about 800 gallons per minute). Aquifer properties, given in column 2 of Table 1, are characteristic of an unconsolidated, sandy formation. The two aquitards have identical properties as listed in column 3 of

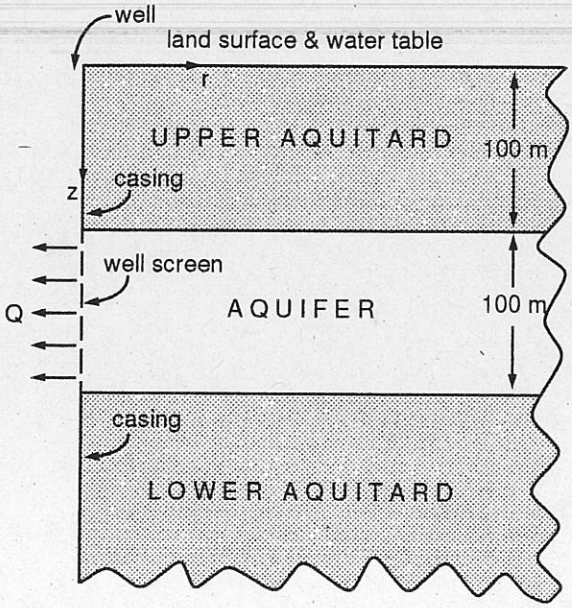

Fig. 1. Hypothetical setting of an aquifer confined above and below by aquitards.

Table 1. Aquitard properties are characteristic of an unconsolidated silty deposit. If the properties in Table 1 are used in a conventional ground-water analysis, (3) would yield an aquifer vertical matrix compressibility, α, of 1.1×10^{-9} m^2/N, which is 2.5 times water compressibility at standard conditions, and the specific storage, given by

$$S_s = \rho_f g\,(\alpha + n\beta) \qquad (4)$$

would be 1.2×10^{-5} m^{-1}. The vertical matrix compressibility of the aquitards is 10 times greater than that of the aquifer, and the corresponding specific storage is 1.1×10^{-4} m^{-1}.

In the numerical model, the aquifer and aquitards extend laterally from the well radius of 0.1 m to an outer boundary 10 km away. The outer boundary is impervious and there is no change in applied stresses. The lower aquitard extends vertically to a bottom boundary 10 km below land surface. The bottom boundary is impervious and there is no displacement. These two remote boundaries are sufficiently distant from the well screen that slight variations in boundary conditions would not affect the solution in the region affected by pumping. The top boundary (land surface) is free of applied forces and is free to deform—in theory of mechanics, this is known as a traction-free boundary. The water table (also at land surface) is approximated as a hydraulic boundary of constant head—as noted above, drawdown of the water table is assumed negligible. At the well, there is no radial displacement and no change in the vertical component of boundary traction. This boundary condition allows the matrix along the well screen/casing to move vertically but not horizontally. A uniform flux of water is withdrawn over the entire thickness of the aquifer, whereas no flow crosses the casing in the aquitards. The 10-km by 10-km model domain is discretized into a 40-column by 100-row mesh of rectangular elements with variable sizes. To prevent numerical oscillation, elements as thin as 0.1 m are used along aquifer-aquitard interfaces. The first time step is 15 seconds, and this time step size is successively increased by 1.2 times until a total simulation time of 50 days is reached.

Figure 2a shows a 300-m by 300-m vertical section of aquifer and aquitards in their initial, undeformed state (prior to pumping). The well is on the left, land surface is at the top, and only the upper 100 m of the lower aquitard is shown. Horizontal and vertical grid lines, spaced 20 m apart, are superimposed on the section. By moving with the skeletal matrix, these grid lines illustrate the deformation of the aquifer and aquitards during pumping. Note that the grid shown in Figure 2a is not the finite-element mesh used in the numerical model.

Figure 2b shows the simulated deformation of the aquifer and aquitards after 10 minutes of pumping. For the sake of illustration, displacements are exaggerated 40,000 times so that, for example, a displacement of 40 m in Figure 2b corresponds to an actual displacement of 1 mm. Contraction of the aquifer is evident. Horizontal contraction in the vicinity of the well is seen as deflection of vertical grid lines towards the screen. A point initially at A in Figure 2a has moved about 0.1 mm in the horizontal direction to A' in Figure 2b. Vertical contraction can be seen in a decrease of aquifer thickness. Immediately adjacent to the well, the decrease of thickness is about 1 mm. It is evident that the aquitards have also deformed. Near the well, the aquitards have contracted in the horizontal direction and extended in the vertical direction, and shear distortion increases towards the aquifer-aquitard interface. The horizontal contraction and shear distortion are similar to those conceptualized by Wolff (1970b). The vertical extension is similar to the "bowing" action conceptualized by Ferris et al. (1962).

The horizontal contraction and vertical extension in the aquitards cause local changes of pore volume. In some parts of the aquitard, pore volume increases. In other parts, pore volume decreases. Understanding the relation between pore volume change and head change is the key to understanding deformation-induced effects. During early time after start of pumping, there is essentially no fluid flow in the aquitards. Under this condition (referred to as "undrained" in poroelasticity terminology), change in hydraulic head is inversely proportional to change in pore volume. At any point in the aquitard, if deformation results in

Table 1. Values of Physical Properties Used in Poroelasticity Simulations

Physical property	*Value in pumped aquifer*	*Value in aquitards*	*Value in unpumped aquifers*
K, hydraulic conductivity (m/s)	1×10^{-4}	1×10^{-7}	1×10^{-5}
G, shear modulus (N/m^2)	3×10^{8}	3×10^{7}	3×10^{8}
ν, drained Poisson's Ratio (dimensionless)	0.25	0.25	0.25
n, porosity (dimensionless)	0.30	0.40	0.30
β, fluid compressibility (m^2/N)	4.4×10^{-10}	4.4×10^{-10}	4.4×10^{-10}

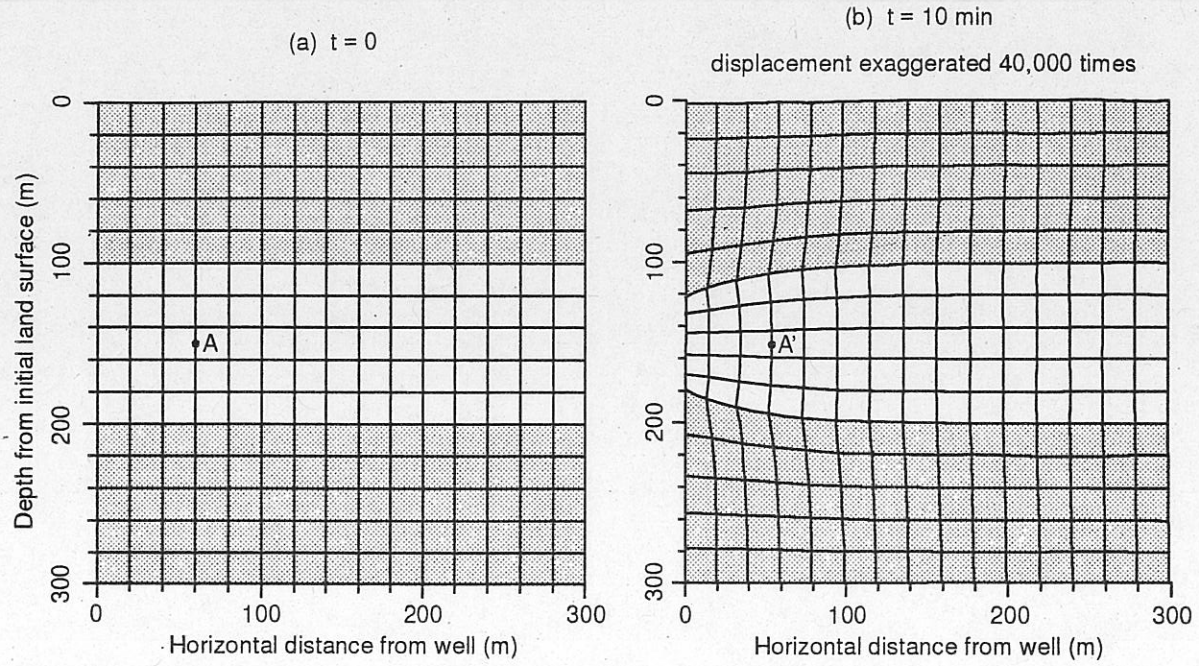

Fig. 2. Deformation of a 300-m by 300-m vertical section of aquifer and aquitards with grid lines superimposed. Unshaded area indicates aquifer. Shaded area indicates aquitard. (a) Initial state. (b) After 10 minutes of pumping.

a net increase in pore volume, hydraulic head drops. Conversely, if deformation results in a net decrease in pore volume, the hydraulic head rises.

The six panels of Figure 3 show progressive changes of hydraulic head in the 300-m by 300-m vertical section of aquifer and aquitards. Negative values indicate head drop, and positive values indicate head rise. Note that contour intervals are irregular. After 10 minutes of pumping (Figure 3a), two zones of induced head drop have developed, one above the well screen and the other below. Although not shown in the figure, the head drops in both zones are between 0 to 1 cm. These two zones are regions of pore volume increase in the aquitards. There are also two separate, emerging zones of induced head rise in the upper aquitard. The shallower zone is just below land surface and next to the well. The deeper zone occurs at the base of the aquitard and about 50 m radially outward from the well. The zones are the regions of pore volume reduction in the aquitard at early times.

As pumping continues, the aquifer contracts further, inducing greater head changes in the aquitard. The maximum head rise exceeds 3 cm after 1 hour of pumping (Figure 3b), and 6 cm after 6 hours (Figure 3c). Head rise is greater in the upper aquitard than in the lower aquitard. The asymmetry is due to the presence of the land surface, where the lack of shear stress allows more ready deformation of the near-surface material. Of the two zones of head rise noted earlier, the shallower one (just below the land surface) has greatly expanded, while the deeper one has almost merged with the expanding contours. Of the two zones of head drop noted earlier, the one above the well screen has almost disappeared, while the one below the well screen has remained about the same. These results show that, in the present case, the deformation-induced effect is primarily a rise in head in the aquitards. Head drop in the aquitards is confined to a relatively small region above and below the well screen.

Over time, the deformation-induced head rise is dissipated by two mechanisms: fluid flow from regions of higher head to regions of lower head (the latter including the water table), and

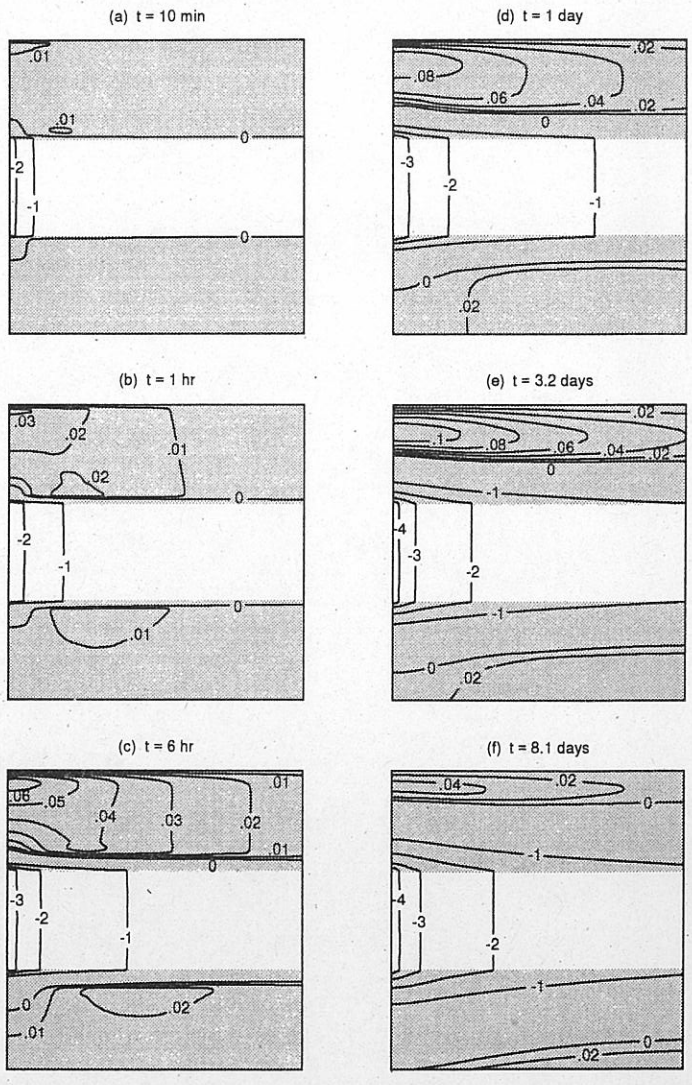

Fig. 3. Changes in hydraulic head, in meters, in a 300-m by 300-m vertical section of aquifer and aquitards. Positive numbers indicate head rise. Negative numbers indicate head drop. Note that contour interval is irregular. Unshaded area indicates aquifer. Shaded area indicates aquitard.

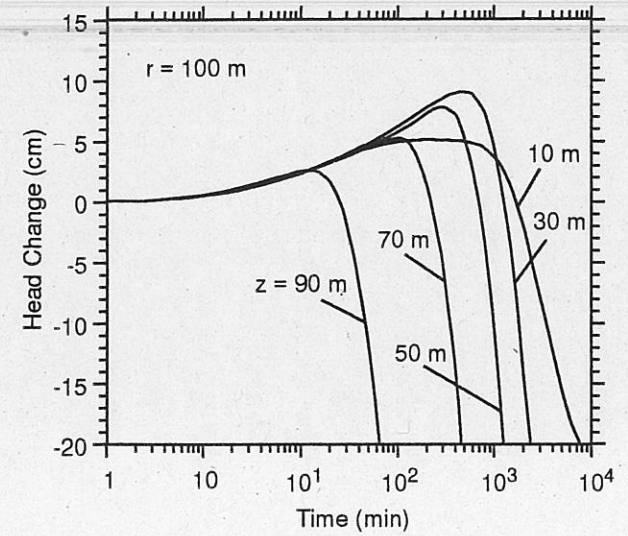

Fig. 4. Plot of head change versus log time at five locations in upper aquitard at a radial distance of 100 m from the pumped well and depths of 10, 30, 50, 70, and 90 m below land surface.

propagation of drawdown from aquifer into aquitard. These processes are illustrated in Figures 3d, e, and f. After one day of pumping, the drawdown front (indicated by the contour of zero head change) has propagated into the lower quarter of the upper aquitard. Above this front, induced head is still increasing (exceeding 8 cm), but flow to the water table has displaced the maximum to a lower position than before. After 3.2 days, the maximum head rise exceeds 10 cm, but the region of head rise in the upper aquitard now encompasses only its upper half. By 8.1 days, the maximum head rise has dropped to about 4 cm, indicating significant dissipation of deformation-induced effects. After 14 days (not shown), drawdown has propagated throughout the upper aquitard, and deformation-induced effects are no longer observable.

Figure 4 shows head change versus log time in the upper aquitard at a radial distance (r) of 100 m from the well and at depths (z) of 10, 30, 50, 70, and 90 m below land surface. The early time rise in head corresponds to deformation-induced effects, whereas the subsequent decline corresponds to the propagation of drawdown from aquifer into aquitard. Near the aquifer-aquitard interface (z = 90 m), the head rise peaks at about 2 cm and lasts for several hours. At a greater distance from the interface (z = 70, 50, and 30 m), the peak is larger and head rise persists longer. However, as the water table is approached (z = 10 m), the peak lessens due to dissipation to the water table. Overall, the results suggest that deformation-induced effects could last for days in a thick aquitard.

Factors that influence deformation-induced effects can be examined by varying model parameters in the poroelasticity simulations. Two sets of results are presented below. The first examines the generation of induced heads. The second examines the dissipation of induced heads. Because the drained Poisson's ratio of unconsolidated sedimentary materials typically falls within a narrow range, it is not varied in the following analysis.

The five panels in Figure 5 show the influence of aquitard thickness and shear modulus (G) on generation of induced heads after one hour of pumping. Figure 5a is the base case and is identical to Figure 3b. Figures 5b and c show head changes when the thickness of the upper aquitard is respectively halved and doubled. Compared to the base case, induced head rise is greater in the thinner aquitard, and less in the thicker aquitard. The thinner aquitard magnifies the influence of land surface, allows greater horizontal compression, and therefore enhances induced head rise at early times. In the thicker aquitard, the induced head change is almost a mirror image of that in the lower aquitard. Figures 5d and e show head changes when the shear moduli of both aquitards are respectively halved and doubled. Compared to the base case, induced head rise is greater in a more rigid aquitard (higher G), and less in a less rigid aquitard (lower G). A more rigid aquitard undergoes less shear deformation near the aquifer-aquitard interface. This allows greater transfer of horizontal forces from the aquifer into the aquitard, resulting in greater head rise. Induced effects at early times are insensitive to hydraulic conductivity of the aquitards.

The five panels in Figure 6 show the influence of hydraulic conductivity and shear modulus on the dissipation of induced heads after 3.2 days of pumping. Figure 6a is the base case and is identical to Figure 3e. Figures 6b and c show head changes when hydraulic conductivities of both aquitards are halved and doubled. Lower hydraulic conductivity causes slower dissipation of induced heads and slower propagation of drawdown from the pumped aquifer. Conversely, higher hydraulic conductivity

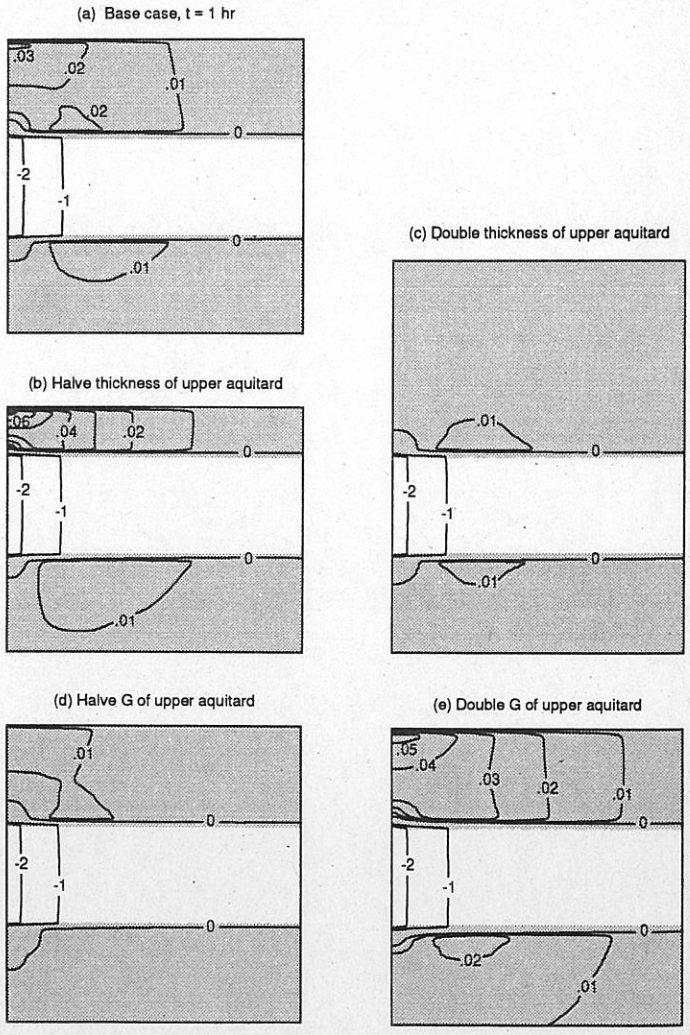

Fig. 5. Changes in hydraulic head, in meters, in a 300-m by 300-m vertical section of aquifer and aquitards after one hour of pumping. The five panels illustrate influence of aquitard thickness and shear modulus on induced effects. Unshaded area indicates aquifer. Shaded area indicates aquitard.

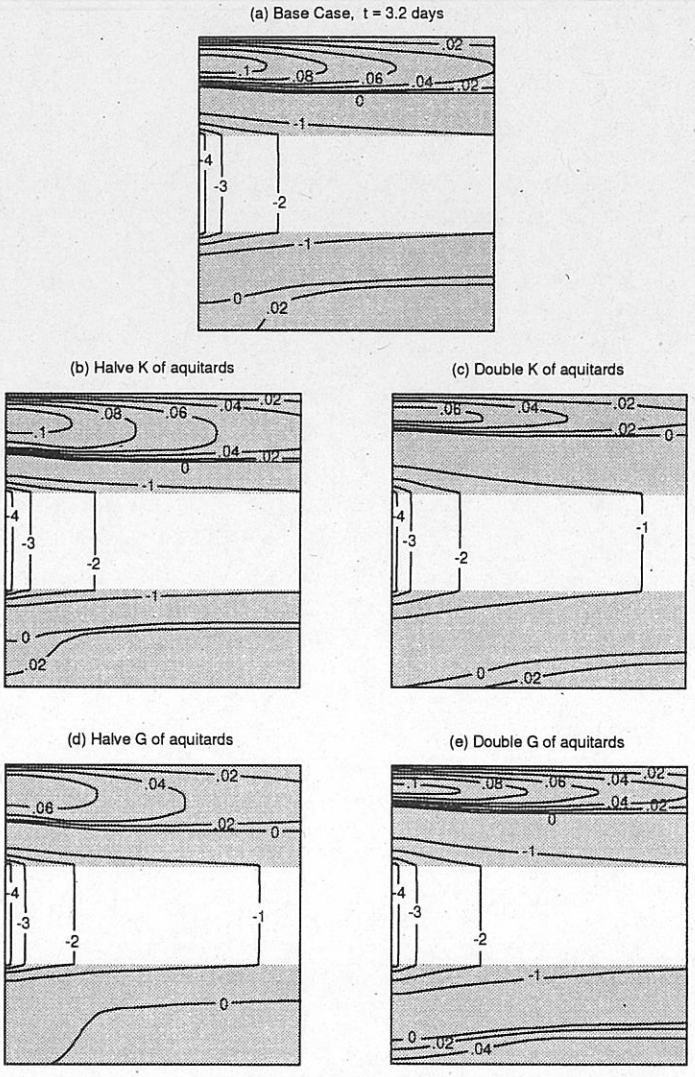

Fig. 6. Changes in hydraulic head, in meters, in a 300-m by 300-m vertical section of aquifer and aquitards after 3.2 days of pumping. The five panels illustrate influence of aquitard hydraulic conductivity and shear modulus on induced effects. Unshaded area indicates aquifer. Shaded area indicates aquitard.

causes faster dissipation of induced head and faster propagation of drawdown from the pumped aquifer. Figures 6d and e show head changes when shear moduli of both aquitards are halved and doubled (with hydraulic conductivity held constant). For head propagation, decreasing the shear modulus has a similar effect to that expected if the specific storage is increased. That is, a lower shear modulus causes slower propagation of heads. However, as noted earlier, a lower shear modulus also causes less induced head rise at early times. These two factors explain why in Figure 6d, induced head rise is less than that in the base case, but drawdown from the pumped aquifer has not propagated as far into the aquitards. Conversely, in Figure 6e, induced head rise is greater then that in the base case, but drawdown from the pumped aquifer has propagated further into the aquitards.

Deformation-Induced Effects in Unpumped Aquifers

The deformation that causes head changes in aquitards can also cause head changes in unpumped aquifers adjacent to the pumped aquifer. Figure 7 shows a hypothetical system of three aquifers, each 100 m thick, separated from one another by 20-m thick aquitards. The upper boundary of the top aquifer is a water table, which coincides with the land surface. The middle aquifer is the pumped aquifer. The bottom aquifer rests on a thick aquitard that extends to a great depth. Properties of the pumped aquifer and all aquitards are same as before (see columns 2 and 3 of Table 1). The two unpumped aquifers have the same properties as the pumped aquifer except their hydraulic conductivities are 10 times less (see column 4 of Table 1).

Pumping rate and boundary conditions for this simulation are the same as those of the previous simulation. The aquifers and aquitards again extend laterally to a distance of 10 km from the well, and the base aquitard extends vertically to a depth of 10 km below land surface. The simulated domain is discretized by a mesh of 40 by 166 rectangular elements of variable sizes. The first time step is 2.5 sec, and this time step size is successively increased by 1.2 times.

Figure 8a shows a 300-m wide by 400-m deep vertical section of the multiple-aquifer-aquitard system in its undeformed state. Superimposed on the section are horizontal and vertical grid lines spaced 20 m apart. Figure 8b shows the simulated deformation, exaggerated 40,000 times, after 10 minutes of pumping. As in the previous simulation (Figure 2b), the pumped aquifer has contracted both in the horizontal and vertical directions. In the present case, the deformation of surrounding layers is concentrated in the thin aquitards, which are less rigid than the unpumped aquifers.

The six panels of Figure 9 show progressive changes in hydraulic head in the 300-m wide by 400-m deep vertical section. Compared to the previous simulation (Figure 3), deformation-induced effects develops faster in the present simulation due to the overall greater rigidity of overlying and underlying layers. After two minutes of pumping, two relatively large zones of induced head drop have developed next to the well, one above and the other below the pumped aquifer. Head drop in these zones ranges from 0 to about 4 cm. There are also two emerging zones of head rise, one just below the land surface, the other

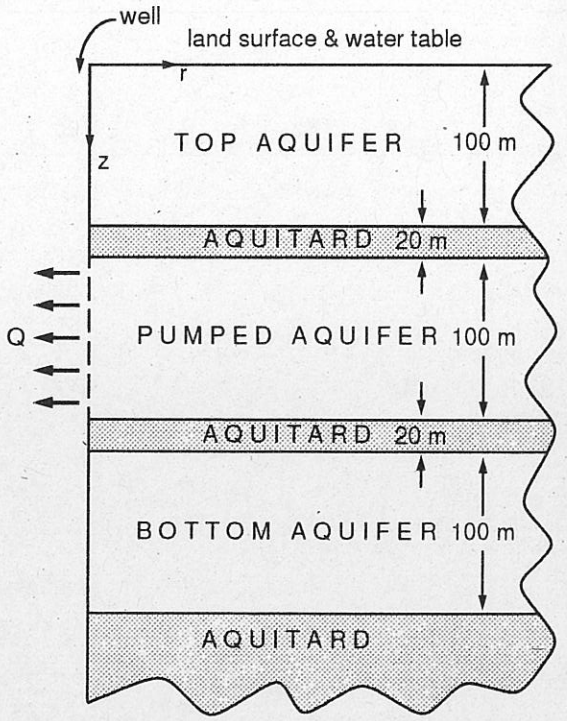

Fig. 7. Hypothetical setting of a multiple-aquifer-aquitard system.

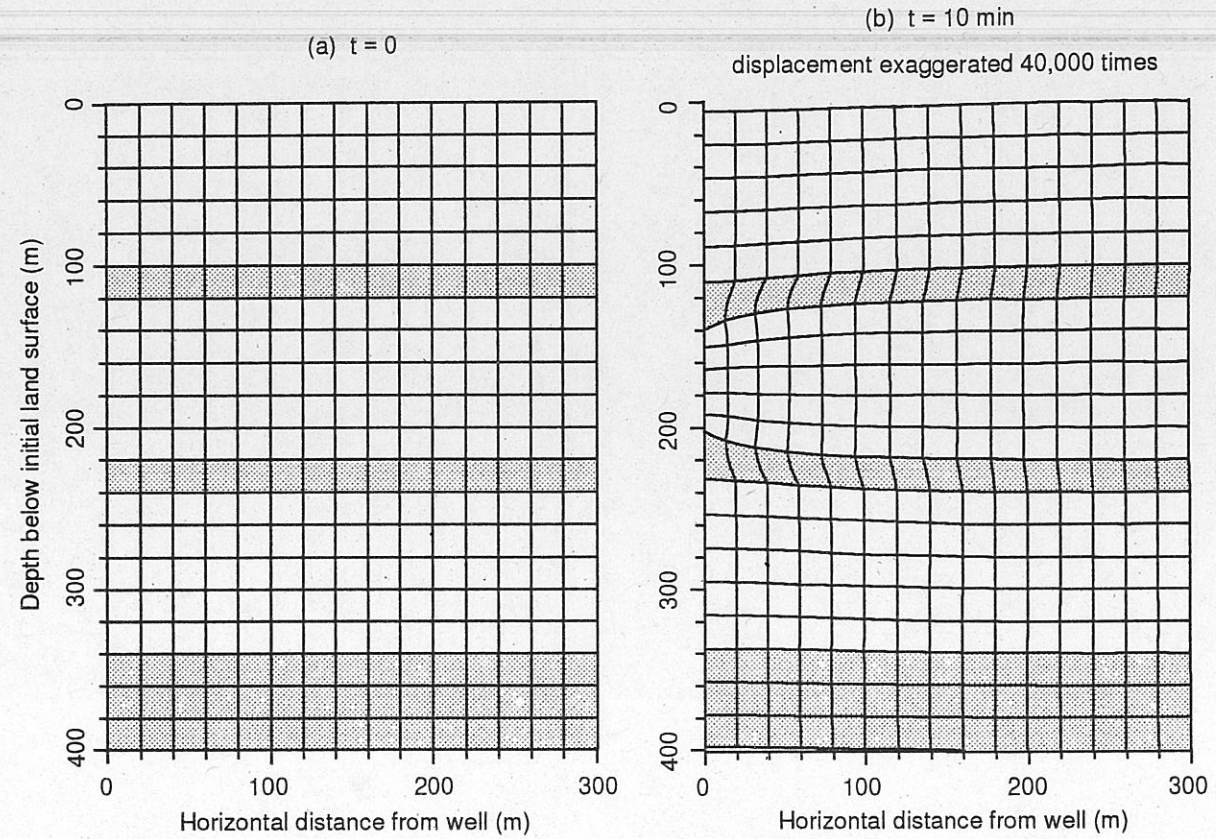

Fig. 8. Deformation of a 300-m wide by 400-m deep vertical section of the multiple-aquifer-aquitard system with grid lines superimposed. Unshaded area indicates aquifer. Shaded area indicates aquitard. (a) Initial state. (b) After 10 minutes of pumping.

just above the base of the bottom aquifer. After 6.4 minutes of pumping, induced head rise is also noticeable in the two thin aquitards. Note that the induced head changes are nearly symmetrical about the pumped aquifer. This occurs because the lower boundary of the bottom aquifer rests on a less rigid aquitard. The deformation of this boundary is similar to that of the land surface.

The relatively high hydraulic conductivity of the unpumped aquifers means that induced head changes are quickly dissipated. After five hours of pumping, the two zones of induced head drop have been obliterated by the surrounding regions of induced head rise. The maximum head rise in the entire simulation does not exceed 3 cm. Dissipation is greater in the top aquifer than in the bottom aquifer due to the presence of the water table. The uneven dissipation also disrupts the early time symmetry. After one day of pumping, deformation-induced head changes are no longer observable.

Deformation-induced effects can impart an interesting oscillation in hydraulic head. Figure 10 shows head change versus log time in the bottom aquifer at a radial distance of 10 m from the well and at depths of 10, 30, 50, 70, and 90 m below the aquifer top (or equivalently, at depths of 250, 270, 290, 310, and 330 m below land surface). Near the top of the bottom aquifer (z = 250 m), the hydraulic head initially declines due to induced head drop in the near-well region. However, as induced head rise develops in the surrounding region, the hydraulic head recovers and actually rises above the prepumping level. Eventually, propagation of drawdown from the pumped aquifer causes the final decline in hydraulic head. At deeper locations in the aquifer (z = 310 and 330 m), the initial drop in hydraulic head is not observed.

Conclusions

The analysis in this study shows that if aquifers and aquitards behave as linearly elastic porous media, then three-dimensional deformation caused by ground-water withdrawal from confined or semiconfined aquifers could induce observable hydraulic head changes in adjacent aquifers and aquitards. These deformation-induced effects occur almost immediately after start of pumping, and include both head rise and head drop. Simulations using a numerical poroelasticity model with typical aquifer and aquitard properties yield induced head changes that range from several centimeters to over 10 centimeters. These results are consistent with reported field observations. Although general conclusions cannot be drawn from a limited number of simulations, results of this study suggest that induced head drop is likely to be observed close to the pumped well in an underlying or overlying aquifer that is separated from the pumped aquifer by a relatively thin aquitard. In contrast, induced head rise is more prominent in an aquitard that extends from land surface to a shallow pumped aquifer. Induced head changes might last for minutes to hours in an aquifer or a relatively thin aquitard, but could persist for many days in a thick aquitard. Induced head changes are eventually dissipated by fluid flow from regions of higher head to regions of lower head, and by propagation of drawdown from the pumped aquifer into adjacent layers.

References

Andreason, G.E. and J.W. Brookhart. 1963. Reverse water-level fluctuations. In: Methods of Collecting and Interpreting Ground-Water Data. Edited by R. Bentall. U.S. Geological Survey Water-Supply Paper 1544-H. pp. 30-35.

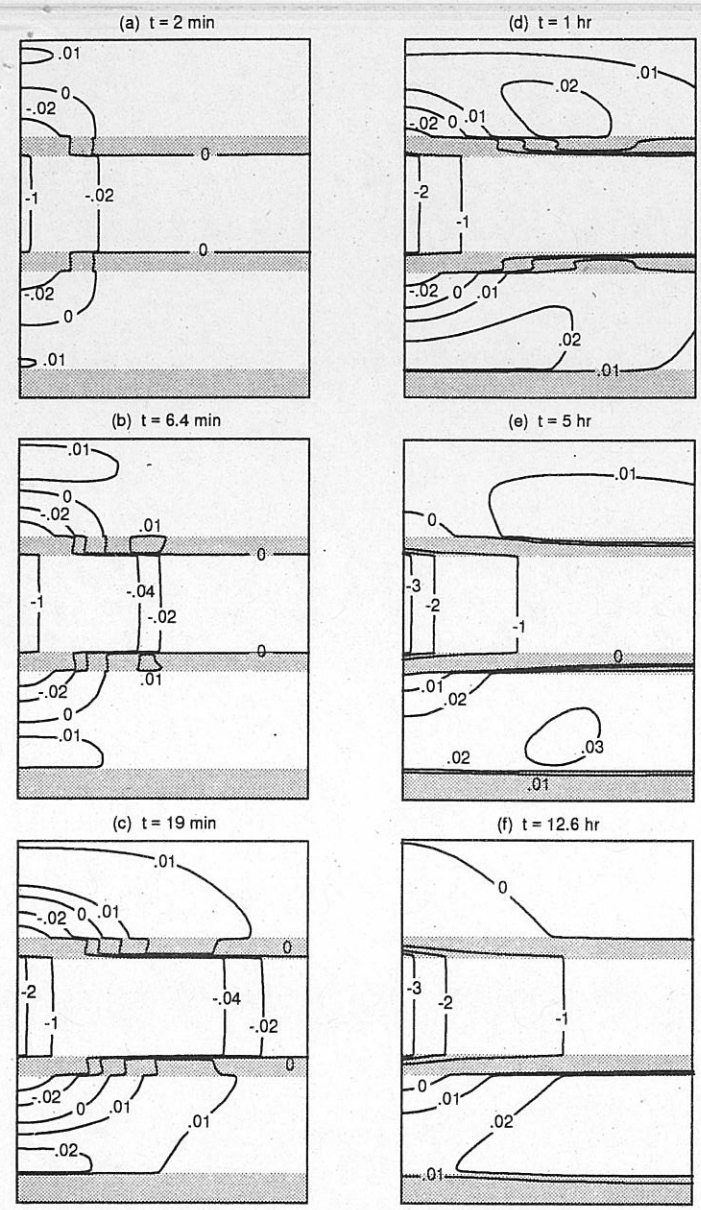

Fig. 9. Changes in hydraulic head, in meters, in a 300-m wide by 400-m deep vertical section of aquifer and aquitards. Positive numbers indicate head rise. Negative numbers indicate head drop. Note that contour interval is irregular. Unshaded area indicates aquifer. Shaded area indicates aquitard.

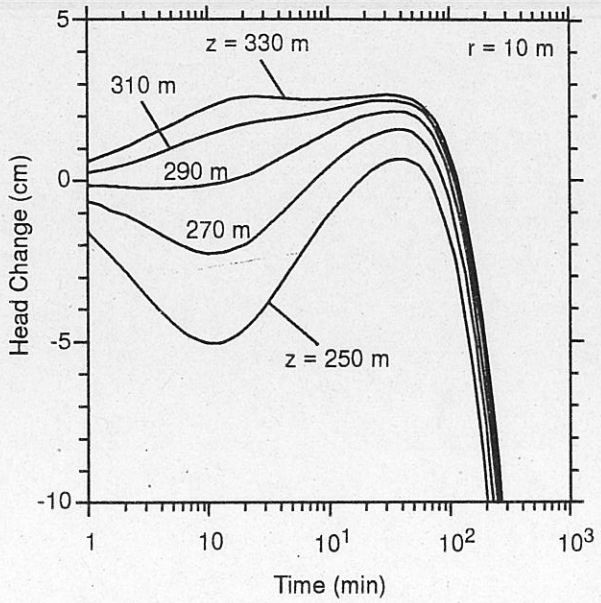

Fig. 10. Plot of head change versus log time at five locations in bottom aquifer at a radial distance of 10 m from the pumped well and depths of 250, 270, 290, 310, and 330 m below land surface.

Biot, M.A. 1941. General theory of three-dimensional consolidation. Journal of Applied Physics. v. 12, pp. 155-164.

Detournay, E. and A. H-D. Cheng. 1993. Fundamentals of poroelasticity. In: Comprehensive Rock Engineering: Principles, Practice and Projects. Edited by J. A. Hudson. Pergamon Press. v. 2, ch. 5.

Ferris, J.G., D.B. Knowles, R.H. Brown, and R.W. Stallman. 1962. Theory of Aquifer Tests. U.S. Geological Survey Water-Supply Paper 1536-E.

Freeze, R.A. and J.A. Cherry. 1979. Groundwater. Prentice-Hall, Englewood Cliffs, NJ.

Gambolati, G. 1974. Second-order theory of flow in three-dimensional deforming media. Water Resources Research. v. 10, pp. 1217-1228.

Geerstma, J. 1973. Land subsidence above compacting oil and gas reservoirs. Journal of Petroleum Technology. v. 25, pp. 734-744.

Gibson, R.E., R.L. Schiffman, and S.L. Pu. 1970. Plane strain and axially symmetric consolidation of a clay layer on a smooth impervious base. Quarterly Journal of Mechanics and Applied Mathematics. v. 23, pp. 505-520.

McNamee, J. and R.E. Gibson. 1960. Plane strain and axially symmetric problems of consolidation of a semi-infinite clay stratum, Quarterly Journal of Mechanics and Applied Mathematics. v. 13, pp. 210-227.

Sandhu, R.S. 1979. Modeling land subsidence. In: Evaluation and Prediction of Subsidence. Edited by S.K. Saxena. American Society of Civil Engineers. p. 565-579.

Schiffman, R.L., A. T-F. Chen, and J.C. Jordan. 1969. An analysis of consolidation theories. Journal of the Soil Mechanics and Foundations Division. Proceedings of the American Society of Civil Engineers. v. 95, pp. 285-312.

Smith, I.M. and D.V. Griffiths. 1988. Programming the Finite Element Method. 2nd ed. John Wiley and Sons, Chinchester.

Verruijt, A. 1969. Elastic storage of aquifers. In: Flow Through Porous Media. Edited by R.J.M. De Wiest. Academic Press, New York. pp. 331-376.

Wolff, R.G. 1970a. Field and laboratory determination of the hydraulic diffusivity of a confining bed. Water Resources Research. v. 6, pp. 194-203.

Wolff, R.G. 1970b. Relationship between horizontal strain near a well and reverse water level fluctuation. Water Resources Research. v. 6, pp. 1721-1728.